DOI: 10.1002/ejic.201000981

Synthesis and Characterization of Novel Guanidine Ligands Featuring Biphenyl or Binaphthyl Backbones

Astrid Maronna,[a] Elvira Bindewald,[a] Elisabeth Kaifer,[a] Hubert Wadepohl,[a] and Hans-Jörg Himmel*[a]

Keywords: Platinum / Coordination modes / Guanidine / Biaryl compounds

In this paper we report on the synthesis and characterization of several new 2,2′-bisguanidino-1,1′-biphenyl and -binaphthyl ligands as well as the electron donor 3,3′,4,4′-tetrakis(tetramethylguanidino)-1,1′-biphenyl. Chiral bisguanidine ligands were prepared with binaphthyl backbones. The solid-state structures were analysed by single-crystal X-ray diffraction. UV/Vis and Raman spectra provided a qualitative insight into the rotational barriers in solution and in the solid state. Finally, late-transition-metal complexes of two of these ligands were prepared. These complexes prefer a κ^1 rather than a κ^2 coordination mode. The discussion of the experimental results is complemented by quantum chemical (DFT) calculations. Finally, we report on the first catalytic test reactions.

Introduction

Asymmetric catalysis is a very active field of research with enormous significance for the manufacture of pharmaceuticals, animal health products, agrochemicals, fungicides and other high-value products. Ligand design is a key issue in the development of new chiral complexes for homogeneous catalysts. One of the most attractive molecules in this context is binap [2,2′-bis(diphenylphosphanyl)-1,1′-binaphthyl].[1,2] Applications, for example, of binap–Ru^{II} dicarboxylate complexes in asymmetric hydrogenations or of cationic binap–Rh complexes in the asymmetric isomerization of allylic amines are well documented.[1] The first attempts to synthesize binap stereospecifically starting with optically pure 2,2′-diamino-1,1′-binaphthyl turned out not to be practical due to racemization at an intermediate stage.[3] Routes involving optical resolution starting with racemic 2,2′-disubstituted 1,1′-binaphthyls were therefore developed. One of the characteristics of binap systems is the large degree of flexibility in the torsional angle between the two naphthyl groups of the binaphthyl backbone.

The suitability of guanidines, especially chiral bicyclic derivatives, in metal-free asymmetric catalysis has already been demonstrated.[4] At the same time, guanidines and guanidinates are well established versatile ligand systems.[5–12] However, surprisingly little is known about the suitability of metal complexes of guanidines in asymmetric catalysis. One example is the Zn–guanidine–amine complex shown in Scheme 1,[13] which has been employed in asymmetric nitroaldol reactions.[14] Guanidines are much stronger bases than amines [e.g., pK_A = 13.6 for $HN=C(NH_2)_2$][15] and can form not only strong σ bonds, but also π bonds to metal ions.[16] Therefore it would be interesting to test the performance of transition-metal complexes of 2,2′-bisguanidine-substituted 1,1′-binaphthyls and related systems in asymmetric catalysis. An interesting point is that the guanidino group, although sterically demanding, leaves enough free space at the imino N atom to allow coordinative bonding to a metal ion. An informative example is provided by the proton sponge 1,8-bis(tetramethylguanidino)naphthalene.[17] In contrast to the corresponding bis(dimethylamino)naphthalene,[18] which is barely suitable as a chelating ligand (only one complex is known to date[19]), we have shown that 1,8-bis(tetramethylguanidino)naphthalene exhibits an interesting and rich coordination chemistry.[20]

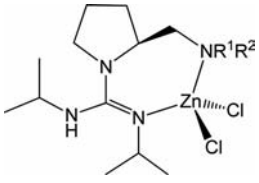

Scheme 1.

Herein we report on the synthesis of achiral bisguanidines with a biphenyl backbone and chiral bisguanidines with a binaphthyl backbone. In addition, we present the first biphenyl with four guanidino substituents. This mole-

[a] Anorganisch-Chemisches Institut, Ruprecht-Karls-Universität Heidelberg,
Im Neuenheimer Feld 270, 69120 Heidelberg, Germany
Fax: +49-6221-545707
E-mail: hans-jorg.himmel@aci.uni-heidelberg.de

Supporting information for this article is available on the WWW under http://dx.doi.org/10.1002/ejic.201000981.

cule is a new member of a class of electron-donor compounds and redox-active ligands recently developed by our group that feature at least four guanidino groups attached directly through the imino N atom to aromatic systems and are referred to as GFAs (guanidino-functionalized aromatic compounds).[21–24] Representatives already known include 1,2,4,5-tetrakis(tetramethylguanidino)benzene (ttmgb),[21] the related (but in its reactivity, remarkably different) compound 1,2,4,5-tetrakis(*N*,*N*′-dimethyl-*N*,*N*′-ethyleneguanidino)benzene (tdmegb)[23] and 1,4,5,8-tetrakis(tetramethylguanidino)naphthalene (ttmgn;[24] see Scheme 2). Quantum chemical calculations indicate that in the gas-phase ttmgb is an even stronger electron donor than bis(imidazolylidene)-tetraazafulvalene,[25] which was recently praised as "organic sodium".[26]

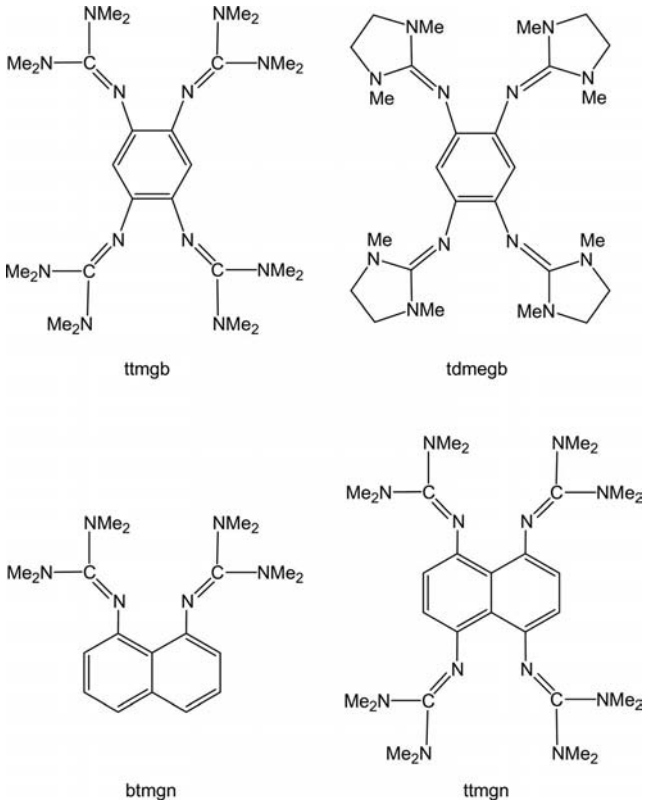

Scheme 2.

Results and Discussion

In the following we report on the synthesis of the new guanidine ligands **1**–**5** shown in Scheme 3. The central C–C single bond, which is common to all these ligands, allows flexibility due to a low rotational barrier. Although achiral molecules result for **1**, **2** and **5** with a biphenyl backbone, **3** and **4** with a binaphthyl backbone are chiral molecules. Subsequently, we discuss some preliminary aspects of the coordination chemistry of some of these new guanidine ligands.

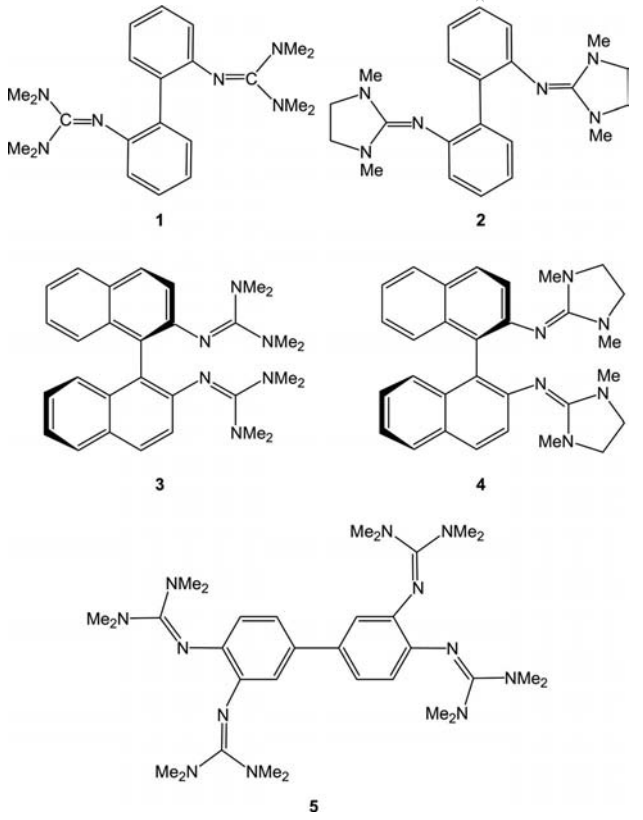

Scheme 3.

Ligand Synthesis and Structural Characterization

All the ligands were synthesized starting with the corresponding amines and *N*,*N*,*N*′,*N*′-tetramethylurea or *N*,*N*′-dimethyl-*N*,*N*′-ethyleneurea. The ureas were activated with oxalyl chloride (to give Vilsmeier salts) prior to reaction with the amines. In contrast to the situation for binap, chiral 2,2′-bisguanidino-substituted 1,1′-binaphthyls can be synthesized in this way starting from optically pure 2,2′-diamino-1,1′-binaphthyl (binam) by stereospecific synthesis. Although the synthesis of **2**–**5** has not previously been described, 2,2′-bis(tetramethylguanidino)-1,1′-biphenyl (**1**) has already been reported in the literature.[27] However, only the diprotonated ligand $[\mathbf{1}H_2]^{2+}$ and not the neutral one was structurally characterized. In our experiments we succeeded in the crystallization and structural characterization of all five neutral molecules. The structures are visualized in Figures 1, 2, and 3. As anticipated, the two phenyl or naphthyl units in the crystallized ligands **1**–**4** are not coplanar. The torsional angles were determined to be around 55° in **1**, 53° in **2**, 66° in **3** and 67° in **4**. For comparison, the torsional angle between the two twisted phenyl planes of biphenyl in its lowest-energy form measures 44.4 ± 1.2°.[28] The increase in the torsional angle in all the guanidine ligands relative to biphenyl reflects the steric demands of the two guanidino groups in the *ortho* positions. Interestingly, the two phenyl rings in solid **5** (*ortho* positions not substituted) are copla-

nar. The C–C bond length connecting the two phenyl or naphthyl units is slightly longer in compounds **2** [149.4(2) pm] and **4** [149.1(2) pm], which feature *N*,*N*′-dimethyl-*N*,*N*′-ethyleneguanidino substituents, than in compounds **1** [148.8(2) pm], **3** [148.9(3) pm] and **5** [148.6(4) pm], which feature tetramethylguanidino substituents. The imino N=C bond lengths in all the ligands fall into the range typical of guanidino groups [129.03(12)/129.45(13) pm in **1**, 128.85(18)/128.45(18) pm in **2**, 130.58(3)/129.3(2) pm in **3**, 127.5(2)/129.6(2) in **4** and 128.8(3)/129.2(3) pm in **5**].

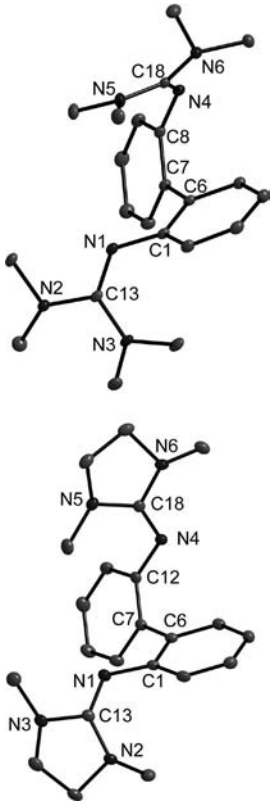

Figure 1. Molecular structures of **1** and **2**. Vibrational ellipsoids drawn at the 50% probability level. Selected bond lengths [pm] and bond angles [°] for **1**: N1–C2 140.18(13), N1–C1 129.03(12), N2–C13 138.89(12), N3–C13 137.82(12), N4–C8 140.30(13), N4–C18 129.45(13), N5–C18 137.48(12), N6–C18 138.53(13), C1–C2 140.90(13), C6–C7 148.88(13), C7–C8 141.42(13), C1–N1–C13 121.74(8), C8–N4–C18 122.60(8), N2–C13–N3 113.83(8), N5–C18–N6 114.40(9), C1–C2–C7–C12 –55.3(9). Selected bond lengths [pm] and bond angles [°] for **2**: N1–C1 140.29(18), N1–C13 128.85(18), N2–C13 138.41(18), N3–C13 138.69(18), N4–C12 141.34(17), N4–C18 128.45(18), N5–C18 138.67(18), N6–C18 138.51(17), C1–C6 140.98(19), C6–C7 149.4(2), C7–C12 140.5(2), C1–N1–C13 122.69(13), N2–C13–N3 108.01(11), C12–N4–C18 120.33(12), N5–C18–N6 108.40(12), C1–C6–C7–C8 –52.8(6).

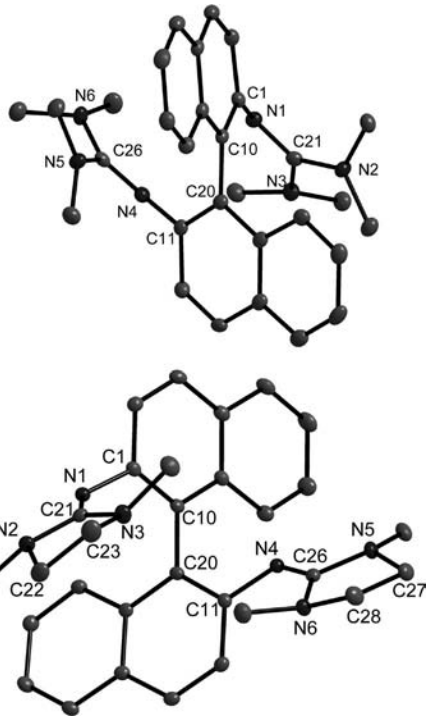

Figure 2. Molecular structures of **3** and **4**. Vibrational ellipsoids drawn at the 50% probability level. Selected bond lengths [pm] and bond angles [°] for **3**: C1–N1 139.3(3), N1–C21 130.5(3), N2–C21 137.4(3), N3–C21 137.9(3), N4–C11 140.7(3), N4–C26 129.3(3), N5–C26 137.8(3), N6–C26 137.9(3), C1–C10 140.0(3), C10–C20 148.9(3), C11–C20 138.2(4), C1–N1–C21 124.8(2), N2–C21–N3 114.8(2), C11–N4–C26 124.5(2), N5–C26–N6 114.4(2), C1–C10–C20–C11 –65.9(11). Selected bond lengths [pm] and bond angles [°] for **4**: N1–C1 139.9(2), N1–C21 127.5(2), N2–C21 139.0(2), N3–C21 138.2(2), N4–C11 139.5(2), N4–C26 129.6(2), N5–C26 136.9(2), N6–C26 138.5(2), C1–C10 139.3(2), C10-C20 149.1(2), C11–C20 139.6(2), C1–N1–C21 128.14(15), N2–C21–N3 108.39(14), C11–N4–C26 124.91(14), N5–C26–N6 108.35(15), C1–C10–C20–C19 66.8(7).

UV/Vis Spectra of the Free Ligands

UV/Vis spectra were recorded for all five ligands in CH_3CN solution (see Exp. Sect.). They provide some insight into the dynamic behaviour of the molecules in solution. The UV/Vis spectrum of biphenyl contains three intense absorption areas at around 170, 190 and 220–280 nm.[29] The relatively broad absorption bands in the region 220–280 nm are usually attributed to resonance interactions involving the two benzenoid rings and consequently the introduction of *ortho* substituents onto the biphenyl brings about dramatic changes in its spectrum (especially with respect to the extinction coefficients).[30] Figure 4 (a) shows the UV/Vis spectra of **1** (two guanidino substituents *ortho* to the central C–C bond) and **5** (four guanidino substituents *meta* and *para* to the central C–C bond). Whereas the spectrum of **1** features bands near 216 and 274 nm, the spectrum of **5** is characterized by three absorptions centred at 217, 270 and 339 nm. Most importantly, the extinction coefficients are much higher for **5** than for **1**. The reason for this difference is that for **1** but not **5**, the degree of freedom of rotation around the central C–C bond is restricted due to the presence of guanidino substituents at the *ortho* positions. The UV/Vis spectra of **2** and **4** (both featuring the same guanidino substituents but different backbones) in the region 200–550 nm are displayed in Figure 5. The extinction coefficients for these two compounds are similar, which suggests a similar degree of rotational freedom. Two

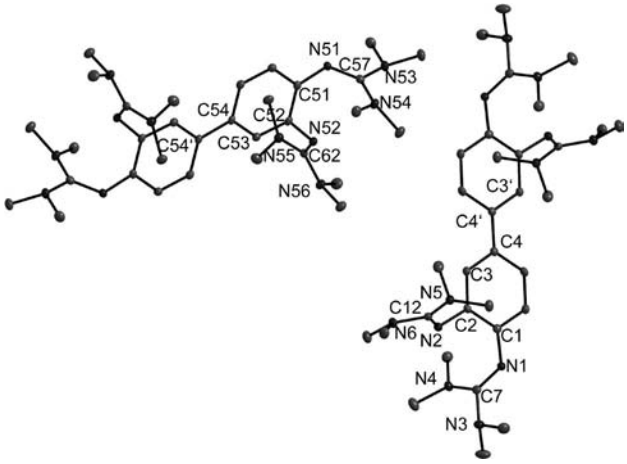

Figure 3. Molecular structure of **5**. Vibrational ellipsoids drawn at the 50% probability level. Selected bond lengths [pm] and bond angles [°]: N1–C1 140.0(3), N1–C7 128.8(3), N2–C2 141.4(3), N2–C12 129.2(3), N3–C7 140.1(3), N4–C7 137.0(3), N5–C12 138.2(3), N6–C12 137.6(3), C1–C2 140.4(3), C2–C3 139.2(3), C3–C4 139.6(3), C4–C4′ 148.6(4), C1–N1–C7 123.02(19), C2–N2–C12 118.77(19), N3–C7–N4 112.97(19), N5–C12–N6 114.46(19), C3–C4–C4′–C3′ 180.00(6), N51–C51 140.3(3), N51–C57 129.2(3), N52–C52 141.0(3), N52–C62 128.8(3), N53–C57 138.4(3), N54–C57 137.2(3), N55–C62 137.4(3), N56–C62 138.8(3), C51–C52 141.1(3), C52–C53 138.9(3), C53–C54 139.5(3), C54–C54′ 148.5(4), C51–N51–C57 122.86(19), C52–N52–C62 120.39(18), N53–C57–N54 114.34(19), N55–C62–N56 114.11(19), C53–C54–C54′–C53′ 180.00(6).

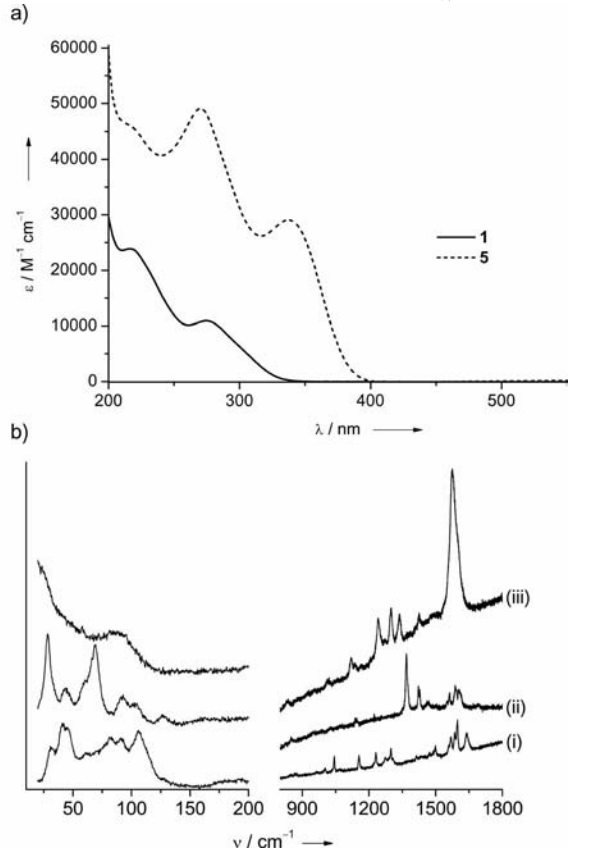

Figure 4. a) UV/Vis spectra of **1** and **5**. b) Raman spectra of (i) **2**, (ii) **4** and (iii) **5** (excited with the 415 nm line of an Ar^+ ion laser, 100–300 mW).

absorption maxima are visible in the spectrum of **2** (Figure 5, a), with the absorption maxima (210 and 275 nm) only slightly shifted with respect to **1**. In the spectrum of **4** (Figure 5, b), four absorption bands are clearly visible at around 214, 265, 305 and 353 nm (shoulder). Of these, the band at 265 nm seems to show some fine structure with maxima at 262 and 268 nm. For comparison, the spectrum of 1,1′-binaphthyl shows an intense absorption band at around 220 nm and a weaker band containing some vibrational structure at around 290 nm.[31] The UV/Vis spectrum of **3** is displayed in the Supporting Information, together with that of **1**. It is similar to that of **4**, with absorption maxima at 214, 255, 304 and 351 nm (shoulder).

Raman Spectra of the Free Ligands

The low-energy vibrations of biphenyls and binaphthyls in the ground and excited electronic states have been intensively studied in the past because there is a correlation between them and the torsional barriers.[32,33] For example, the torsional mode of 1,1′-binaphthyl has been shown to occur at around 30 cm^{-1}. In the case of biphenyl in its ^1A ground electronic state, quantum chemical [B3LYP/6-31G(d)] calculations yielded frequencies of 71, 96, 129 and 271 cm^{-1} for the torsional and other inter-ring vibrational modes.[32] In our experiments, the spectra were excited with the 514 nm line of an Ar^+ ion laser. This excitation energy is well below the energy needed for the electronic excitations responsible for the absorptions observed in the UV/Vis spectra. Therefore we performed the measurements under non-resonance conditions. Nevertheless, the solid samples showed signs of beam damage after prolonged exposure to the laser beam. In particular, in the Raman spectra of **1** and **3** (see the Raman spectrum of **1** in the Supporting Information), broad and large fluorescence signals are observed. Therefore only the Raman spectra of **2**, **4** and **5**, some parts of which are shown in Figure 4 (b), will be discussed herein. In the case of the ligands **2** and **4**, in which rotation is restricted due to the guanidino groups at the *ortho* positions, we observed sharp signals in the low-energy region of the Raman spectra [at 28.5, 43.5, 68.8 (with a shoulder at 59.9), 91.9, 103.6 and 126.6 cm^{-1} for **4** and 31.3, 41.1/44.9, 82.0, 91.4 and 106.0 cm^{-1} for **2**]. On the other hand, the spectrum of **5** shows a single very broad signal at around 88 cm^{-1}. A second broad feature was centred out of the range of detection at around 20 cm^{-1}.

CV Curves and Redox Chemistry

Biphenyl has a relatively high oxidation potential, around 2 V versus SCE.[34] The situation changes upon the introduction of two guanidino substituents. However, the waves are generally broad and non-reversible (see, for example, the CV curves recorded for **2** and **4** in the Supporting Information). As anticipated, the introduction of four gua-

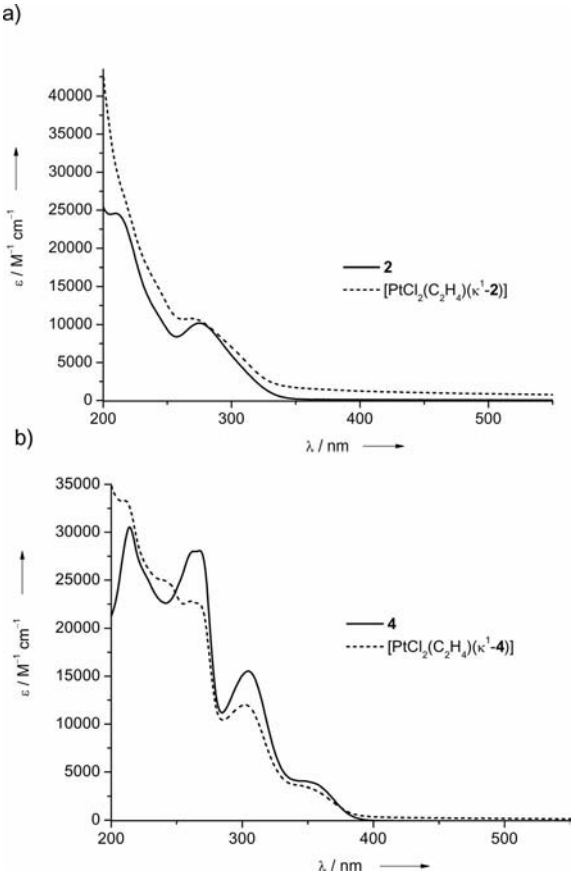

Figure 5. UV/Vis spectra of a) **2** and $[PtCl_2(C_2H_4)(\kappa^1\text{-}\mathbf{2})]$ and b) **4** and $[PtCl_2(C_2H_4)(\kappa^1\text{-}\mathbf{4})]$.

nidino substituents in **5** has the greatest impact on the oxidation potential. The CV curve of **5** features two reversible oxidation/reduction waves located at $E_{1/2}$ = 0.06 and 0.61 V (see Figure 6, a). Measurements in the presence of ferrocene in solution indicate that both peaks can be assigned to one-electron oxidation/reduction. Upon two-electron oxidation, the central C–C bond is transformed from a single to a double bond [see the Lewis structure in Equation (1)]. Guanidino groups at the *para* or *ortho* positions assist this oxidation and could stabilize the positive charges. In addition, gas-phase oxidation was analysed with the aid of quantum chemical (B3LYP/6-311G**) calculations. The calculated gas-phase structure of the dication $\mathbf{5}^{2+}$ is illustrated in the Supporting Information. The calculations show a reduction in the central C–C bond length from 148.4 pm in neutral **5** to 142.4 pm in $\mathbf{5}^{2+}$. Upon oxidation, the aromaticity is removed from the two C_6 rings, leading to C–C bond lengths in the range 138.7–148.0 pm. We also tried to oxidize **5** chemically by reaction with I_2. Upon addition of I_2 to a CH_3CN solution of **5**, the reaction mixture immediately turned dark green. The NMR spectra indicate the presence of a mixture of products. The UV/Vis spectrum (see the Supporting Information) shows bands at 290 and 353 nm assignable to the I_3^- anion, which indicates that a redox reaction indeed has taken place. In addition, a broad band appears at 705 nm, which is responsible for the intense colour of the solution and was assigned to oxidized

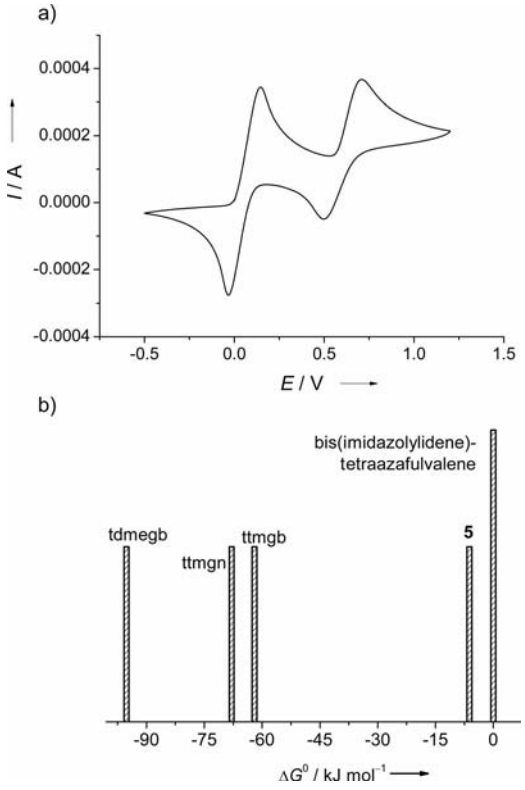

Figure 6. a) CV curve [SCE, 100 mV s^{-1}, CH_3CN, (nBu$_4$N)(PF_6) as electrolyte] for **5**. b) Gas-phase donor strength of several GFAs measured relative to bis(imidazolylidene)tetraazafulvalene on the basis of the model electron-transfer reaction [bis(imidazolylidene)-tetraazafulvalene]$^{2+}$ + GFA → bis(imidazolylidene)tetraazafulvalene + $[GFA]^{2+}$.

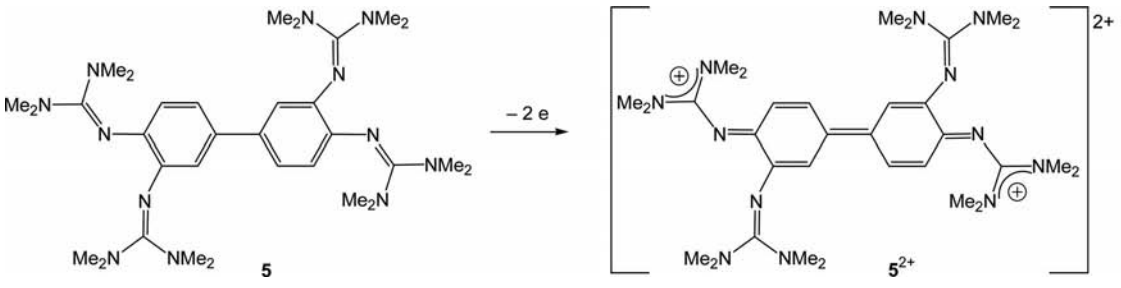

(1)

5. In Figure 6 (b) the calculated two-electron gas-phase donor capacity of **5** is compared with that of other aromatic compounds featuring four guanidino substituents and of the "organic sodium" bisimidazolylidene-tetraazafulvalene on the basis of the ΔG^0 value of the redox reaction shown in Equation (2). According to these calculations, compound **5** is a slightly better electron donor than the tetraazafulvalene in the gas phase. However, it exhibits a lower donor capacity than the three tetrakisguanidine compounds ttmgb, tdmegb and ttmgn (see Scheme 1 for their Lewis formula).

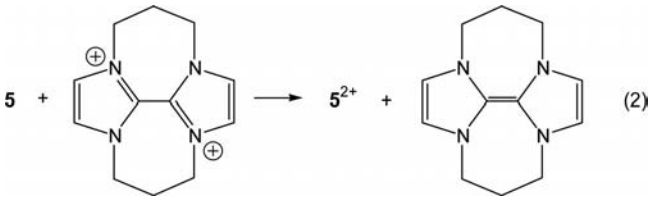

Coordination Chemistry and Preliminary Catalytic Tests

When **2** was allowed to react with Zeise's dimer, $[Pt_2Cl_4(C_2H_4)_2]$, the formation of a new product was detected by NMR spectroscopy. In the ^{195}Pt NMR spectrum, a single signal is observed at –2849 ppm. Figure 7 (a) shows the ^1H NMR spectra of **2** before and after the reaction.

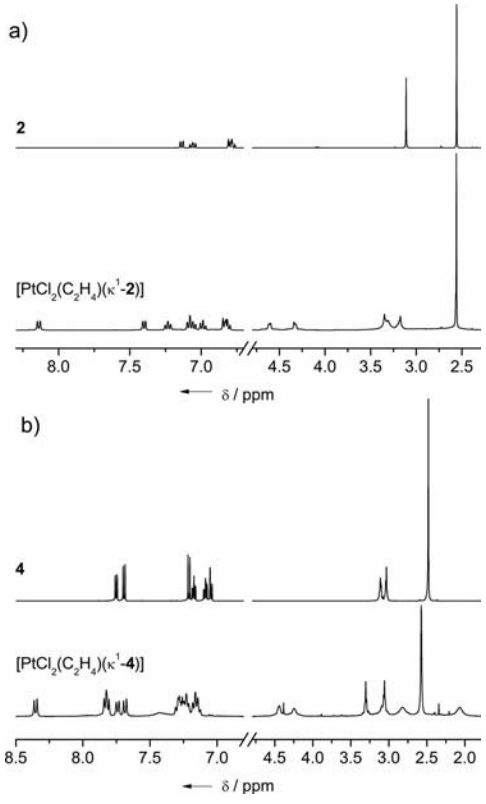

Figure 7. ^1H NMR spectra recorded for CD_2Cl_2 solutions of a) **2** and the complex $[PtCl_2(C_2H_4)(\kappa^1\text{-}\mathbf{2})]$ (400 MHz) and b) **4** (600 MHz) and the complex $[PtCl_2(C_2H_4)(\kappa^1\text{-}\mathbf{4})]$ (400 MHz).

Signals at around 4.6 and 4.3 ppm (the latter showing coupling to Pt) directly indicate the presence of an ethylene ligand in the product. The number of signals in the aromatic region signals the formation of an unsymmetrical product. In line with the other analytical data, the peaks in the FAB^+ mass spectrum suggest the formation of the complex $[PtCl_2(C_2H_4)(\kappa^1\text{-}\mathbf{2})]$. The product was crystallized and studied by XRD. Figure 8 (a) shows its molecular structure. Ligand **2** is indeed κ^1-coordinated to Pt^{II}, *trans* to the ethylene ligand, in the same way as already reported for $[PtCl_2(C_2H_4)(\kappa^1\text{-}\mathbf{1})]$.[20] As anticipated, the imino N=C bond length within the coordinating guanidino group increases to 132.8(4) pm upon coordination and is significantly longer than that of the non-coordinating guanidino group [129.2(4) pm]. The Pt–N bond measures 207.5(2) pm and compares with a value of 206.9(4) pm measured in the related complex $[PtCl_2(C_2H_4)(\kappa^1\text{-btmgn})]$ (see Scheme 4). The torsional angle between the two phenyl rings is around 53°, as in free **2**. In the crystalline phase, dimeric assemblies are formed through two Pt–Cl···H–C contacts of around 261.7(5) pm (see Figure 8, b).

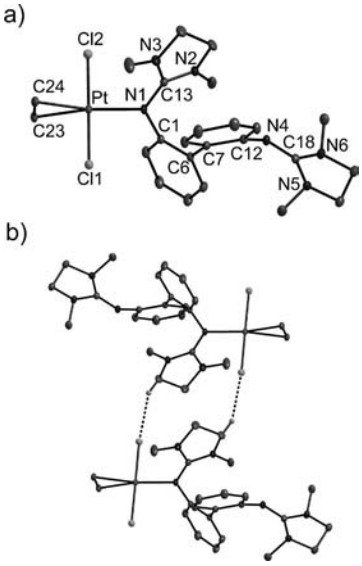

Figure 8. a) Molecular structure of the complex $[PtCl_2(C_2H_4)(\kappa^1\text{-}\mathbf{2})]$. Vibrational ellipsoids drawn at the 50% probability level. Selected bond lengths [pm] and bond angles [°]: Pt–N1 207.5(2), Pt–Cl1 229.48(9), Pt–Cl2 229.52(9), Pt–C23 214.1(3), Pt–C24 213.9(3), N1–C1 142.8(4), N1–C13 132.8(4), N2–C13 133.8(4), N3–C13 135.2(4), N4–C12 140.1(4), N4–C18 129.2(4), N5–C18 139.0(4), N6–C18 138.0(4), C1–C6 140.7(4), C6–C7 149.4(4), C7–C12 141.9(4), Cl1–Pt–N1 90.63(8), Cl2–Pt–N1 89.71(8), Pt–N1–C1 117.14(19), Pt–N1–C13 123.9(2), N2–C13–N3 108.8(3), N1–C1–C6 123.0(3), C1–C6–C7 122.3(3), C6–C7–C12 122.0(3), N4–C12–C7 120.8(3), C12–N4–C18 122.5(3), N4–C18–N5 130.1(3), N4–C18–N6 121.4(3), N5–C18–N6 108.5(2), C1–C6–C7–C8 52.9(17). b) Molecular structure of the dimeric assembly of complex $[PtCl_2(C_2H_4)(\kappa^1\text{-}\mathbf{2})]$.

According to our analytical data (see the Exp. Sect.), the reaction between (*R*)-**4** and $[Pt_2Cl_4(C_2H_4)_2]$ proceeds similarly to that between **2** and $[Pt_2Cl_4(C_2H_4)_2]$. The ^1H NMR spectra obtained for **4** before and after reaction are

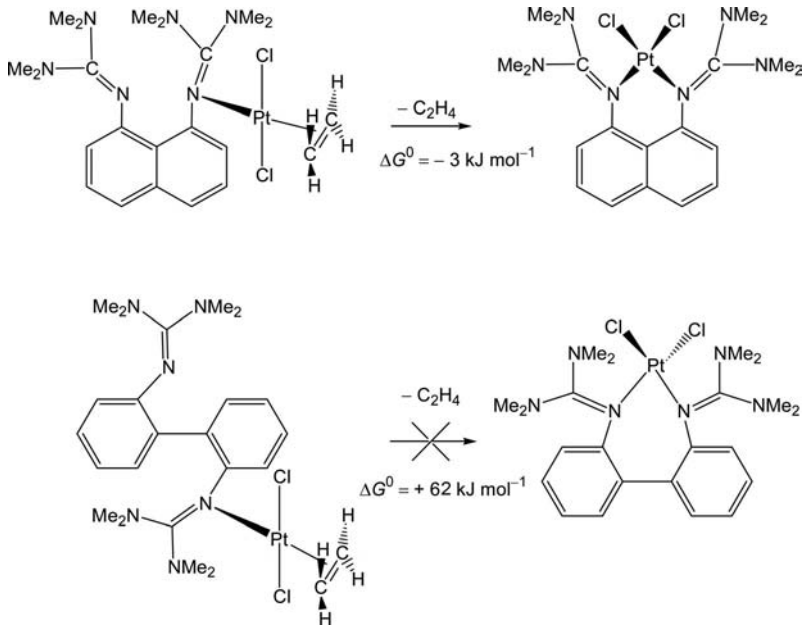

Scheme 4.

Table 1. Calculated (B3LYP/LANL2DZ) bond lengths and wavenumbers of the two ν(C=C) + δ(CH_2) vibrational modes for the compounds discussed in this work.

Compound	*d*(C=C) [pm]	*d*(Pt–Cl) [pm]	*d*(Pt–N) [pm]	*d*(C=N) [pm]	ν(C=C) + δ(CH_2) [cm^{-1}]
C_2H_4	134.8	–	–	–	1677.6/1387.5
$[Pt_2Cl_4(C_2H_4)_2]$	142.6	238.2/249.1	–	–	1544.3, 1543.4/1251.3, 1250.4
$[PtCl_2(C_2H_4)(\kappa^1$-**2**$)]$	141.1	244.2/243.4	208.4	130.2 (free), 134.8 (coord.)	1550.4/1279.1
$[PtCl_2(C_2H_4)\{(R)$-κ^1-**4**$\}]$	141.1	244.2/243.4	208.5	130.0 (free), 135.0 (coord.)	1548.9/1277.3

shown together in Figure 7b. Again the presence of a C_2H_4 ligand in the product can be deduced from the signals at around 4.4 and 4.2 ppm. The high-resolution FAB^+ mass spectrometric data also point to the formation of the complex $[PtCl_2(C_2H_4)\{(R)$-κ^1-**4**$\}]$. Unfortunately the crystals obtained for this species turned out to be of insufficient quality for an XRD analysis. The gas-phase structure derived from quantum chemical calculations is illustrated in the Supporting Information (see Table 1 for a list of selected properties).

We also recorded the Raman spectra. Unfortunately, the spectra recorded for $[PtCl_2(C_2H_4)(\kappa^1$-**4**$)]$ suffered from visible beam damage. Figure 9 shows the spectra obtained for ligand **2** and the corresponding complex $[PtCl_2(C_2H_4)$-$(\kappa^1$-**2**$)]$ (the complete spectra are shown in the Supporting Information.). Two signals at 1501 and 1236 cm^{-1} (see Figure 9, a) were assigned to modes that can be described as mixtures predominantly of ν(C=C) and $\delta_s(CH_2)$.[35–37] In the IR spectrum a band at 1502 cm^{-1} is observed (see the Supporting Information). A problem with any attempt at correlating the observed wavenumbers with the properties of the Pt–C_2H_4 bond is that the potential energy distribution changes significantly and almost unpredictably in ethylene–metal complexes. For example, in the $[PtCl_3(C_2H_4)]^-$ complex anion, the character of the higher-energy mode (now at 1516 cm^{-1}) is 21% ν(C=C) and 36% δ(CH_2), and for the lower-energy mode (at 1230 cm^{-1}) 76% ν(C=C) and 10% δ(CH_2).[38] Powell et al. suggested a simple method for comparing the bonding in ethylene complexes.[39] In this method, the summed percentage lowering of ν(C=C) and $\delta_s(CH_2)$ is a measure of the decrease of the double bond character of the olefin upon coordination. The summed percentage is 15.4% in the case of $[PtCl_2(C_2H_4)(\kappa^1$-**2**$)]$ [with 1623 and 1342 cm^{-1} for ν(C=C) and $\delta_s(CH_2)$ in free ethylene]. This value is significantly higher than that derived for standard *trans*-$[PtCl_2(C_2H_4)L]$ complexes (for example, with L a pyridine derivative or CH_3CN).[40] In previous work on Ni^{II} complexes we showed that the guanidino N–metal bond exhibits a strong σ(N→Ni) and a weaker π(N→Ni) donor component,[16] a result that is in line with the presence of strong Pt–C_2H_4 back-bonding. A comparison of some of the calculated bonding parameters for $[PtCl_2(C_2H_4)\{(R)$-κ^1-**4**$\}]$, $[PtCl_2(C_2H_4)(\kappa^1$-**2**$)]$, $[Pt_2Cl_4$-$(C_2H_4)_2]$ and free C_2H_4 in Table 1 also supports this conclusion. Figure 9 (a) also shows the low-energy region of the Raman spectra, which reveals that complex formation affects the torsional and other inter-ring vibrations. Furthermore, the 250–550 cm^{-1} region is shown in Figure 9 (b) and is characteristic of the ν(Pt–Cl), ν(Pt–N) and ν(Pt–C_2) modes. For example, in $(n\mathrm{Bu}_4\mathrm{P})[PtCl_3(C_2H_4)]$, ν(Pt–Cl) and ν(Pt–$C_2$) occur at 338/332/313 and 512 (ν_s)/413 (ν_{as}) cm^{-1}, respectively.[38] In *trans*-$[PtBr_2(NH_2Ph)(C_2H_4)]$, the Pt–N stretching mode, ν(Pt–N), is located at 430 cm^{-1}.[38] In the case of $[PtCl_2(C_2H_4)(\kappa^1$-**2**$)]$, we tentatively assigned the

doublet at 336.4/330.2 cm^{-1} to the two ν(Pt–Cl) modes, the two weak features at 424.7 and 372.5 cm^{-1} to the ν(Pt–C_2) modes and the signal at 396.7 cm^{-1} to the ν(Pt–N) mode.

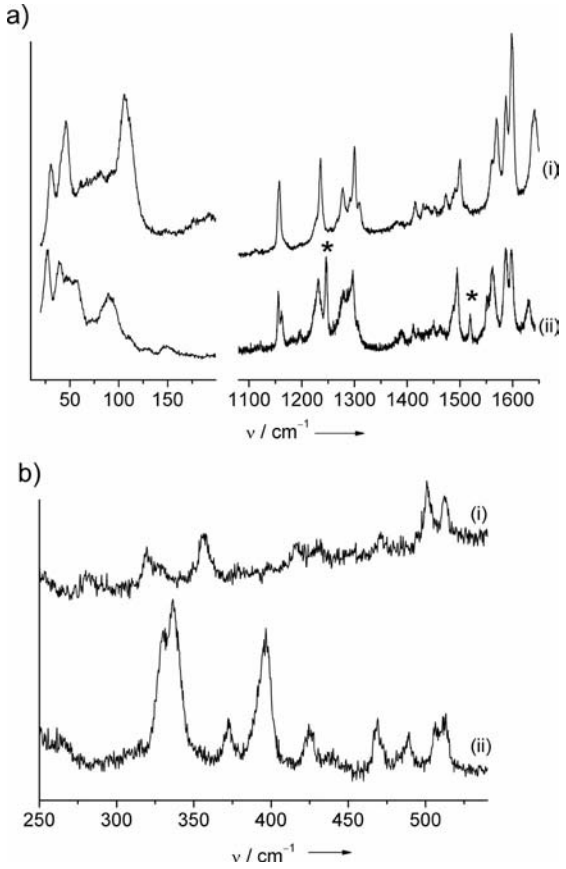

Figure 9. Raman spectra measured for (i) **2** and (ii) [$PtCl_2(C_2H_4)(\kappa^1$-**2**)] excited with the 415 nm line of an Ar^+ ion laser (100–300 mW). a) The low-frequency region (20–200 cm^{-1}) characteristic of torsional and other inter-ring vibrational modes together with the 1100–1650 cm^{-1} region containing the two vibrational modes with high ν(C=C) + $\delta_s(CH_2)$ character (highlighted by asterisks). b) The 250–550 cm^{-1} region containing the ν(Pt–C_2), ν(Pt–Cl) and ν(Pt–N) modes for (i) **2** and (ii) [$PtCl_2(C_2H_4)(\kappa^1$-**2**)].

The complex [$PtCl_2(C_2H_4)(\kappa^1$-btmgn)] (see Scheme 4) was shown to thermally eliminate C_2H_4 in CH_2Cl_2 at reflux to give [$PtCl_2(\kappa^2$-btmgn)].[20] In contrast, the synthesis of [$PtCl_2(\kappa^2$-**1**)] in CH_2Cl_2 at reflux could not be realized. Attempts to eliminate C_2H_4 photolytically in CH_2Cl_2 or toluene also failed. The NMR spectra indicate the formation of a mixture of products, but it was impossible to isolate and/or identify a single product. In the light of these experimental findings, quantum chemical (B3LYP/LANL2DZ) calculations were carried out to compare the thermodynamic properties of the ethylene elimination starting with the two complexes [$PtCl_2(C_2H_4)(\kappa^1$-btmgn)] and [$PtCl_2(C_2H_4)(\kappa^1$-**1**)] (see Scheme 4). In the case of [$PtCl_2(C_2H_4)(\kappa^1$-btmgn)], ΔG^0 (free energy at 298 K, 1 bar) was previously estimated to be –3 kJ mol^{-1}.[20] For [$PtCl_2(C_2H_4)(\kappa^1$-**1**)],[20] a significantly endergonic value was determined (ΔG^0 = +62 kJ mol^{-1}). The calculations are thus in line with the experimental results. According to the quantum chemical calculations, the product of ethylene elimination, [$PtCl_2(\kappa^2$-**1**)], does not exhibit a planar coordination, but a sawhorse-type structure (see the Supporting Information).

Traces of water had to be rigorously excluded in all our experiments. When the Pt^{II} complex [$PtCl_2(C_2H_4)(\kappa^1$-**1**)][20] was dissolved in CD_2Cl_2 and the solution exposed to air to allow reaction with traces of H_2O, a small amount of brown crystalline product precipitated, which turned out to consist of [(**1**H)$PtCl_3$] molecular units. Subject to the very same reaction conditions, red crystals of [(**1**H)$PdCl_3$] were obtained during the attempt to synthesize the neutral Pd^{II} complex with 1,2-cyclooctadiene as olefin moiety. The molecular structures of these products derived from an XRD analysis are provided in the Supporting Information. The flexibility in the torsional angle between the two phenyl ring planes allows significant N–H···Cl–M hydrogen-bonding. Attempts to obtain [(**1**H)$PtCl_3$] in the absence of traces of water starting with [$(NH_4)_2PtCl_4$] failed.

We then tested the catalytic activity of the Pt^{II} complexes. The three complexes [$PtCl_2(C_2H_4)(\kappa^1$-**1**)],[20] [$PtCl_2(C_2H_4)$-(κ^1-**2**)] and [$PtCl_2(C_2H_4)${(*R*)-κ^1-**4**}] were used to catalyse the hydrosilylation reaction between Et_3SiH and Me_3-SiC(H)CH_2 to yield $Et_3SiCH_2CH_2SiMe_3$. For this reaction there are of course already numerous catalysts available. Nevertheless, this reaction was of interest in the context of our study because we have previously shown that Pt dichloride complexes with κ^2-coordinated bisguanidine ligands are catalytically inactive.[20] This implies that ethylene elimination, as shown in Scheme 4, directly affects the TON. If [$PtCl_2(\kappa^1$-bisguanidine)] complexes are formed as intermediates in the catalytic process (whatever species represents the active catalyst and no matter if the catalysis is homogeneous or heterogeneous), they must be very short-lived because isomerization to [$PtCl_2(\kappa^2$-bisguanidine)] most likely extinguishes the catalytic activity.[20] The reaction was followed by GC–MS and the results are shown in Figure 10. All three complexes turned out to be catalytically active. Complex [$PtCl_2(C_2H_4)(\kappa^1$-**2**)] exhibits the smallest turnover frequency (TOF) at the beginning of the reaction, which might signal the presence of an induction period. After

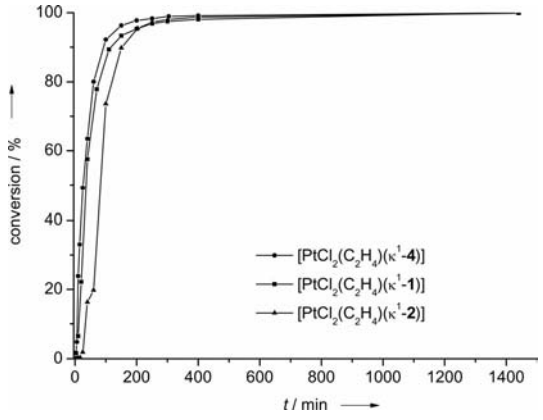

Figure 10. Results of the catalytic hydrosilylation of trimethylsilylethane using the new Pt–guanidine complexes.

250 min the conversion to the product was >95% for all three catalysts. The TOF for the three complexes $[PtCl_2(C_2H_4)(\kappa^1\text{-}\mathbf{1})]$, $[PtCl_2(C_2H_4)(\kappa^1\text{-}\mathbf{2})]$ and $[PtCl_2(C_2H_4)\{(R)\text{-}\kappa^1\text{-}\mathbf{4}\}]$ are around 240, 270 and 190 h^{-1}, respectively (in the time period 20–100 min after the start of the reaction). The experiments thus indicate that $[PtCl_2(\kappa^2\text{-}\mathbf{1})]$, which is likely to be catalytically inactive, is not formed as an intermediate in the course of the reaction.

Conclusions

We have reported herein the synthesis and characterization of several new guanidine ligands with biphenyl and binaphthyl backbones. Preliminary experiments on the coordination chemistry of the bisguanidine systems indicate that they prefer a κ^1 bonding mode instead of a chelating κ^2 bonding mode. Thus, the second guanidino group could act as a hemilabile ligand stabilizing a vacancy at the metal created in the course of a catalytic cycle. Ongoing research in our group includes the use of the chiral binaphthyl ligands **3** and **4** in asymmetric catalysis. In addition, the redox chemistry of the new electron donor **5** will be explored.

Experimental Section

All reactions were carried out under Ar using standard Schlenk techniques. 2,2′-Diamino-1,1′-biphenyl was synthesized as described in the literature.[41] The dinuclear complex di-μ-chloro-dichlorobis(ethylene)diplatinum(II) $[PtCl(C_2H_4)(\mu\text{-}Cl)]_2$ (97%) used in the synthesis of the Pt complexes (*R*)-(+)-2,2′-diamino-1,1′-binaphthyl (99%) and *N*,*N*′-dimethylethyleneurea was purchased from ABCR. Oxalyl chloride, tetramethylurea, acetonitrile and *n*-hexane were used from Aldrich without further purification as well as chloroform purchased from Acros. Other solvents were dried using the standard methods and then distilled. NMR spectra were measured with Bruker Avance II 400 and Avance III 600 spectrometers. A Cary 5000 spectrophotometer was used to record UV/Vis spectra. IR spectra of CsI discs of the compounds were recorded with a FT-IR Biorad Merlin Excalibur FT 3000 spectrometer. GC–MS measurements were performed with an Agilent Technologies G1530A MSD 5973N device. An EG&G Princeton 273 apparatus was used for the CV measurements. Raman spectra were recorded with a T64000 spectrometer from Horiba–Jobin–Yvon. The 514 nm line of an Ar^+ ion laser (100–300 mW) was used for excitation.

1: 2-Chloro-1,1′,3,3′-tetramethylformamidinium chloride (Vilsmeier salt) was prepared by adding oxalyl chloride (7.6 mL, 88 mmol, 16 equiv.) to a solution of *N*,*N*,*N*′,*N*′-tetramethylurea (2.3 mL, 19.3 mmol, 3.5 equiv.) dissolved in $CHCl_3$ (15 mL) at room temperature. The reaction mixture was heated at reflux overnight. After evaporating the solvent, the remaining white solid was washed with Et_2O (2 × 20 mL). Reaction of the synthesized Vilsmeier salt with 2,2′-diamino-1,1′-biphenyl (1.01 g, 5.5 mmol, 1 equiv.) was performed according to the experimental procedure described by Pruszynski et al.[27] Yield 1.44 g (67%). Crystals suitable for X-ray diffraction were obtained by recrystallization from hot *n*-hexane solution. ^{1}H NMR (600.13 MHz, CD_2Cl_2, 295.0 K): δ = 7.06 (t, ^3J = 6.90 Hz, 4 H, CH), 6.77 (t, ^3J = 7.33 Hz, 2 H, CH), 6.64–6.68 (m, 2 H, CH), 2.57 (s, 24 H, CH_3) ppm. ^{13}C NMR (150.90 MHz, CD_2Cl_2, 295.0 K): δ = 158.38, 150.45, 133.56 (C_q), 131.48, 126.94, 122.39, 119.04 (CH), 39.55 (CH_3) ppm. IR (CsI): $\tilde{\nu}$ = 3051 (w), 3011 (w), 2926 (m), 2886 (m), 2801 (w), 1607 (s), 1577 (s), 1498 (m), 1455 (m), 1428 (m), 1374 (s), 1269 (w), 1236 (m), 1203 (w), 1139 (s), 1061 (w), 1017 (s), 925 (w), 860 (w), 783 (m), 758 (m), 737 (s), 702 (w), 623 (w), 566 (w), 521 (w), 502 (w), 463 (w) cm^{-1}. Raman measurements not possible due to laser beam damage (even for 100 mW and short exposure times). UV/Vis (CH_3CN, $c = 2.53 \times 10^{-5}$ mol L^{-1}): λ (ε) = 274 (10946), 218 (23878 L mol^{-1} cm^{-1}) nm. MS (ESI^+): *m*/*z* (%) = 381.27561 (100) $[MH]^+$. $C_{22}H_{32}N_6$ (380.54): C 69.44, H 8.48, N 22.09; found C 69.61, H 8.44, N 22.06.

Crystal data for **1**: $C_{22}H_{32}N_6$, M_r = 380.53, 0.40 × 0.40 × 0.40 mm^3, monoclinic, space group $P2_1/n$, a = 8.0995(5), b = 15.1232(8), c = 17.9918(10) Å, β = 100.2960(10)°, V = 2168.3(2) $Å^3$, Z = 4, $\rho_{calcd.}$ = 1.166 Mg m^{-3}, Mo-K_α radiation (graphite-monochromated, λ = 0.71073 Å), T = 100 K, θ_{range} = 1.77–32.33°. Reflections measured 6006, independent 7353, R_{int} = 0.0557. Final R indices [$I > 2\sigma(I)$]: R_1 = 0.0470, wR_2 = 0.1400.

2: Oxalyl chloride (7 mL, 80 mmol, 20 equiv.) was added dropwise to a solution of 1,3-dimethylethyleneurea (1.7 mL, 16 mmol, 4 equiv.) dissolved in $CHCl_3$ (30 mL) at room temperature. The reaction mixture was stirred under reflux for 20 h. After removal of the solvent in vacuo, the activated urea, 2-chloro-1,3-dimethylethyleneformamidinium chloride, was washed with Et_2O (15 mL). Then the orange solid was redissolved in CH_2Cl_2 (20 mL) and added to a solution of 2,2′-diamino-1,1′-biphenyl (0.74 g, 4 mmol, 1 equiv.) and triethylamine (3.4 mL, 24 mmol, 6 equiv.) in CH_2Cl_2 (30 mL) at 255 K. Subsequently the reaction mixture was warmed to room temperature and after 2 h stirring at room temperature the mixture was extracted with 10% aq. HCl. The aqueous solution was washed with CH_2Cl_2 and after addition of 25% aq. KOH, the solution was extracted with toluene. The combined toluene phases were dried with K_2CO_3 and the solvent was removed in vacuo. The residue was recrystallized from toluene/*n*-hexane to give colourless crystals of **2** (1.16 g, 77%). ^{1}H NMR (399.89 MHz, CD_2Cl_2, 295.3 K): δ = 7.14 (dd, ^3J = 7.50, ^4J = 1.53 Hz, 2 H, 5-H), 7.08–7.04 (m, 2 H, 3-H), 6.79 (ddd, ^3J = 8.66, 5.62, ^4J = 1.94 Hz, 4 H, 2-H/4-H), 3.11 (s, 8 H, CH_2), 2.56 (s, 12 H, CH_3) ppm. ^{13}C NMR (100.56 MHz, CD_2Cl_2, 297.5 K): δ = 154.86 (2 C, C-13/C-18), 148.79 (2 C, C-1/C-12), 133.89 (2 C, C-6/C-7), 131.52 (2 C, C-5/C-8), 126.72 (2 C, C-3/C-10), 122.93(2 C, C-2/C-11), 119.18 (2 C, C-4/C-9), 48.81 (4 C, CH_2), 35.43 (4 C, CH_3) ppm. IR (KBr): $\tilde{\nu}$ = 3053 (m), 3023 (m), 2941 (s), 2859 (s), 2850 (s), 2368 (w), 2340 (w), 1661 (s), 1585 (s), 1560 (m), 1466 (m), 1426 (m), 1390 (m), 1274 (s), 1233 (m), 1139 (w), 1110 (w), 1070 (w), 1031 (m), 964 (m), 862 (m), 768 (s), 732 (s), 701 (m), 650 (m), 587 (m), 506 (s) cm^{-1}. Raman (514 nm, 300 mW): ν = 31.3, 41.1/44.9, 82.0, 91.4, 106.0, 319.9, 356.3, 500.8, 512.7, 550.2, 645.5, 691.9, 724.9, 775.2, 1002.7, 1044.1, 1155.6, 1231.2, 1273.9, 1298.8, 1308.6, 1559.3, 1568.7, 1585.5, 1597.8, 1639.7, 2944.3, 3056.8 cm^{-1}. UV/Vis (CH_3CN, $c = 2.58 \times 10^{-5}$ mol L^{-1}): λ (ε) = 275 (10187), 210(24580 L mol^{-1} cm^{-1}) nm. MS (ESI^+): *m*/*z* (%) = 377.24550 (100) $[MH]^+$. $C_{22}H_{28}N_6$ (376.50): calcd. C 70.18, H 7.50, N 22.32; found C 70.18, H 7.46, N 22.13.

Crystal data for **2**: $C_{22}H_{28}N_6$, M_r = 376.50, 0.40 × 0.30 × 0.25 mm^3, triclinic, space group $P\bar{1}$, a = 9.1410(18), b = 9.934(2), c = 12.142(2) Å, α = 79.57(3), β = 85.82(3), γ = 69.69(3)°, V = 1016.9(3) $Å^3$, Z = 2, $\rho_{calcd.}$ = 1.230 Mg m^{-3}, Mo-K_α radiation (graphite-monochromated, λ = 0.71073 Å), T = 100 K, θ_{range} = 1.71–27.43°. Reflections measured 8637, independent 4620, R_{int} = 0.0293. Final R indices [$I > 2\sigma(I)$]: R_1 = 0.0472, wR_2 = 0.1122.

***(R)*-3:** Oxalyl chloride (5.4 mL, 61.6 mmol, 35 equiv.) was added dropwise to a solution of *N*,*N*,*N*′,*N*′-tetramethylurea (1.5 mL,

12.3 mmol, 7 equiv.) dissolved in $CHCl_3$ (20 mL) at room temperature. The reaction mixture was stirred under reflux for 15 h. After removal of the solvent in vacuo, the remaining solid, 2-chloro-1,1′,3,3′-tetramethylformamidinium chloride, was washed with Et_2O (20 mL). Then the white solid was dissolved in CH_2Cl_2 (20 mL) and added to a solution of (*R*)-(+)-2,2′-diamino-1,1′-binaphthalene (0.5 g, 1.76 mmol, 1 equiv.) and triethylamine (1.5 mL, 10.6 mmol, 6 equiv.) in CH_2Cl_2 (30 mL) at 255 K. The mixture was stirred for a further 1 h at 255 K and subsequently warmed up to room temperature. After stirring for 3 h at room temperature the reaction mixture was extracted with 10% aq. HCl and the aqueous solution was washed with CH_2Cl_2. Then 25% aq. NaOH was added and the solution was extracted with toluene. The combined toluene phases were dried with K_2CO_3 and the solvent was removed in vacuo. The residue was recrystallized from hot *n*-hexane to give (*R*)-**3** (622.0 mg, 73%). ^{1}H NMR (600.13 MHz, CD_2Cl_2, 295.0 K): δ = 7.76 (d, ^3J = 8.06 Hz, 2 H, 5-H/15-H), 7.71 (d, ^3J = 8.71 Hz, 2 H, 3-H/13-H), 7.17 (ddd, ^3J = 8.00, 6.21, ^4J = 1.68 Hz, 2 H, 6-H/16-H), 7.11–7.05 (m, 4 H, 7-H/17-H/8-H/18-H), 6.99 (d, ^3J = 8.71 Hz, 2 H, 2-H/12-H), 2.43 (s, 24 H, CH_3) ppm. ^{13}C NMR (100.56 MHz, CD_2Cl_2, 296.0 K): δ = 158.41(2 C, C-21/C-26), 148.78 (2 C, C-1/C-11), 135.14 (2 C, C-9/C-19), 129.18 (2 C, C-4/C-14), 128.00 (2 C, C-5/C-15), 127.28 (2 C, C-3/C-13), 126.60 (2 C, C-8/C-18), 125.18 (2 C, C-7/C-17), 124.94 (2 C, C-2/C-12), 124.35 (2 C, C-10/C-20), 122.27 (2 C, C-6/C-16), 39.37 (8 C, CH_3) ppm. IR (CsI): $\tilde{\nu}$ = 3045 (m), 3004 (m), 2936 (s), 2882 (s), 2799 (m), 2362 (w), 1601 (s), 1578 (s), 1500 (m), 1454 (w), 1422 (m), 1378 (s), 1316 (w), 1237 (m), 1208 (m), 1140 (s), 1064 (m), 1038 (m), 1021 (m), 976 (m), 952 (w), 915 (w), 860 (w), 825 (s), 756 (s), 739 (s), 683 (w), 652 (m), 616 (w), 572 (m), 534 (m), 486 (m), 427 (m) cm^{-1}. Raman measurements not possible due to laser beam damage (even for 100 mW and short exposure times). UV/Vis (CH_3CN, $c = 3.13 \times 10^{-5}$ mol L^{-1}): λ (ε) = 351 (sh, 3839), 304 (13927), 255 (27278), 214 (28338 L mol^{-1} cm^{-1}) nm. MS (ESI$^+$): *m*/*z* (%) = 482.31070 (33.3) $[M(H)_2]^{2+}$, 481.30731 (100) $[MH]^+$, 383.22298 (63.3) $[MH - C_5H_{10}N_2]^+$. $C_{30}H_{36}N_6$ (480.65): calcd. C 74.97, H 7.55, N 17.48; found C 74.93, H 7.57, N 17.43.

Crystal data for (*R*)-**3**: $C_{30}H_{36}N_6$, M_r = 480.65, $0.40 \times 0.35 \times 0.30$ mm^3, orthorhombic, space group $P2_12_12_1$, a = 14.926(3), b = 15.625(3), c = 11.382(2) Å, α = 90, β = 90, γ = 90°, V = 2654.5(9) Å^3, Z = 4, $\rho_{calcd.}$ = 1.203 Mg m^{-3}, Mo-K_α radiation (graphite-monochromated, λ = 0.71073 Å), T = 100 K, θ_{range} = 1.89–27.48°. Reflections measured 6116, independent 6086, R_{int} = 0.046. Final R indices [$I > 2\sigma(I)$]: R_1 = 0.0564, wR_2 = 0.1239.

(*R*)-4: Oxalyl chloride (1.8 mL, 20 mmol, 20 equiv.) was added dropwise to a solution of 1,3-dimethylethyleneurea (0.4 mL, 4 mmol, 4 equiv.) dissolved in $CHCl_3$ (10 mL) at room temperature. The reaction mixture was stirred at reflux overnight. After removal of the solvent in vacuo, the remaining solid, 2-chloro-1,3-dimethylethyleneformamidinium chloride, was washed with Et_2O (15 mL). Then the orange solid was redissolved in CH_2Cl_2 (10 mL) and added to a solution of (*R*)-(+)-2,2′-diamino-1,1′-binaphthalene (284.4 mg, 1 mmol, 1 equiv.) and triethylamine (0.8 mL, 6 mmol, 6 equiv.) in CH_2Cl_2 (30 mL) at 255 K. The reaction mixture was warmed to room temperature over 6 h and subsequently extracted with 10% aq. HCl. After washing the aqueous solution with CH_2Cl_2, 25% aq. NaOH was added and the solution was extracted with toluene. The combined toluene phases were dried with K_2CO_3 and the solvent was removed in vacuo. The orange residue was washed with *n*-hexane to give (*R*)-**4** (347.2 mg, 73%) as a light-yellow powder. Crystals suitable for X-ray diffraction were obtained by recrystallization from toluene/*n*-hexane. ^{1}H NMR (600.13 MHz, CD_2Cl_2, 295.0 K): δ = 7.75 (d, ^3J = 8.03 Hz, 2 H, 5-H/15-H), 7.69 (d, ^3J = 8.72 Hz, 2 H, 3-H/13-H), 7.21 (d, ^3J = 8.72 Hz, 2 H, 2-H/12-H), 7.19–7.15 (m, 2 H, 6-H/16-H), 7.11–7.07 (m, 2 H, 7-H/17-H), 7.05 (d, ^3J = 8.45 Hz, 2 H, 8-H/18-H), 3.17–2.98 (m, 8 H, CH_2), 2.48 (s, 12 H, CH_3) ppm. ^{13}C NMR (150.90 MHz, CD_2Cl_2, 295.0 K): δ = 155.57 (2 C, C-21/C-26), 147.11 (2 C, C-1/C-11), 134.76 (2 C, C-9/C-19), 129.21 (2 C, C-4/C-14), 127.77 (2 C, C-5/C-15), 126.91 (2 C, C-3/C-13), 126.14 (2 C, C-8/C-18), 125.46 (2 C, C-10/C-20), 125.27 (2 C, C-7/C-17), 124.74 (2 C, C-2/C-12), 122.35 (2 C, C-6/C-16), 48.66 (4 C, CH_2), 35.52 (4 C, CH_3) ppm. IR (CsI): $\tilde{\nu}$ = 3051 (m), 2937 (s), 2841 (s), 1691 (s), 1640 (s), 1607 (s), 1589 (s), 1490 (m), 1442 (w), 1420 (w), 1371 (m), 1279 (m), 1227 (m), 1142 (w), 1075 (w), 1039 (s), 988 (w), 953 (s), 856 (w), 825 (s), 752 (s), 699 (w), 640 (w), 620 (w), 590 (w), 525 (w), 505 (w), 479 (m), 424 (w) cm^{-1}. Raman (514 nm, 300 mW): $\tilde{\nu}$ = 28.5, 43.5, 59.9/68.8, 91.9, 103.6, 126.6, 243.0, 408.6, 428.8, 541.1, 582.4/591.0, 688.5, 849.7, 1138.7, 1144.5, 1368.6, 1422.4, 1428.2, 1562.0, 1589.0, 1608.2 cm^{-1}. UV/Vis (CH_3CN, $c = 2.10 \times 10^{-5}$ mol L^{-1}): λ (ε) = 353 (sh, 3905), 305 (15523), 265 (27980), 214 (30535 L mol^{-1} cm^{-1}) nm. MS (ESI$^+$): *m*/*z* (%) = 477.27627 (100) $[MH]^+$. $C_{30}H_{32}N_6$ (476.62): calcd. C 75.60, H 6.77, N 17.63; found C 75.60, H 6.50, N 17.61.

Crystal data for **(*R*)-4**: $C_{30}H_{32}N_6$, M_r = 476.62, $0.50 \times 0.45 \times 0.40$ mm^3, orthorhombic, space group $P2_12_12_1$, a = 8.0800(16), b = 15.223(3), c = 20.610(4) Å, V = 2535.1(9) Å^3, Z = 4, $\rho_{calcd.}$ = 1.249 Mg m^{-3}, Mo-K_α radiation (graphite-monochromated, λ = 0.71073 Å), T = 100 K, θ_{range} = 1.66–30.04°. Reflections measured 7451, independent 7419, R_{int} = 0.056. Final R indices [$I > 2\sigma(I)$]: R_1 = 0.0489, wR_2 = 0.1129.

5: 3,3′-Diaminobenzidine (1.714 g, 8.00 mmol) was dissolved in CH_3CN (10 mL). Then NEt_3 (14.00 mL) and the activated urea suspended in CH_3CN (30 mL) were added at 0 °C. The red-brown reaction mixture was stirred for a period of 2 h at 0 °C. During removal of the solvent in vacuo a beige precipitate formed, which was filtered off. The solvent was removed from the filtrate and the brown solid residue redissolved in 10% aqueous HCl solution. Then 25% aqueous NaOH solution was added. The pale-brown suspension was extracted with a total amount of Et_2O (80 mL). The combined organic phases were dried with K_2CO_3. Then the solvent was removed in vacuo. Sublimation at 160–170 °C and 2×10^{-2} mbar afforded the product as a white solid. ^{1}H NMR (600 MHz, CD_3CN): δ = 6.91 (dd, ^3J = 7.99, ^5J = 2.22 Hz, 2 H, 6-H/6′-H), 6.60 (d, ^5J = 2.21 Hz, 2 H, 5-H/5′-H), 6.40 (d, ^3J = 7.99 Hz, 2 H, 2-H/2′-H), 2.648/2.649 (d, 48 H, CH_3) ppm. ^{13}C NMR (150 MHz, CD_3CN): δ = 159.16 (C-7/C-7′/C-8/C-8′), 150.08 (C-7/C-7′/C-8/C-8′), 145.26 (C-3/C-3′), 143.67 (C-4/C-4′), 134.39 (C-1/C-1′), 122.57 (C-2/C-2′), 119.71 (C-5/C-5′), 118.69 (C-6/C-6′), 39.80/39.74 (CH_3) ppm. IR (CsI): $\tilde{\nu}$ = 3008 (w), 2931 (w), 2908 (w), 2831 (w), 1612 (m), 1496 (m), 1373 (s), 1242 (w), 1142 (s), 1064 (w), 1018 (s), 925 (w), 871 (w), 817 (m) cm^{-1}. Raman (514 nm, 300 mW): λ = ca. 20, ca. 88, 422.1, 480.6, 675.9, 737.4, 781.6, 833.4, 1013.0, 1119.5, 1136.8, 1241.8, 1299.5, 1337.0, 1426.2, 1575.4, 2930.6 cm^{-1}. UV/Vis (CH_3CN, $c = 6.6 \times 10^{-5}$ mol L^{-1}): λ (ε) = 266 (2.4×10^4), 256 (2.6×10^4 L mol^{-1} cm^{-1}) nm. CV (CH_3CN, SCE, scan speed 100 mV s^{-1}): $E_{½}$ = 0.06, 0.61 V. MS (FAB$^+$): *m*/*z* = 606.5 (50) $[M]^+$, 562.8 (100) $[M - NMe_2]^+$, 517.7 (9) $[MH - (NMe_2)_2]^+$. MS (ESI$^+$): *m*/*z* = 607.5 (98) $[M + H]^+$, 1213.9 (100) $[2M + H]^+$. $C_{32}H_{54}N_{12}$ (606.87): calcd. C 63.33, H 8.97, N 27.70; found C 63.08, H 9.01, N 27.14.

Crystal data for **5**: $C_{32}H_{54}N_{12}$, M_r = 606.87, $0.19 \times 0.13 \times 0.05$ mm^3, monoclinic, space group $P2_1/c$, a = 7.320(4), b = 22.786(14), c = 20.857(11) Å, β = 90.593(12)°, V = 3479(3) Å^3, Z = 4, $\rho_{calcd.}$ = 1.159 Mg m^{-3}, Mo-K_α radiation (graph-

ite-monochromated, λ = 0.71073 Å), T = 100 K, θ_{range} = 1.79–25.03°. Reflections measured 53261, independent 6073, R_{int} = 0.0866. Final R indices [$I > 2\sigma(I)$]: R_1 = 0.0502, wR_2 = 0.1075.

[PtCl$_2$(C$_2$H$_4$)(κ^1-2)]: [PtCl$_2$(C$_2$H$_4$)]$_2$ (117.6 mg, 0.2 mmol, 1 equiv.) dissolved in CH_2Cl_2 (8 mL) was added to a solution of **2** (147.6 mg, 0.39 mmol, 1.96 equiv.) in CH_2Cl_2 (12 mL). The resulting clear yellow solution was stirred for 1 h at room temperature. After removal of the solvent in vacuo, a yellow powder was obtained, which was washed twice with PE (40/60, 8 mL) to give [PtCl$_2$(C$_2$H$_4$)(κ^1-**2**)] (259.0 mg, 98%). Crystals suitable for X-ray diffraction were obtained by slow diffusion of PE (40/60) into a toluene solution of the product. ^{1}H NMR (399.89 MHz, CD_2Cl_2, 295.0 K): δ = 8.14 (d, ^3J = 7.33 Hz, 1 H, 11-H), 7.4 (dd, ^3J = 7.51, ^4J = 1.36 Hz, 1 H, 5-H), 7.23 (dt, ^3J = 8.06, 8.02, ^4J = 1.62 Hz, 1 H, 10-H), 7.11–7.03 (m, 2 H, 8-H/3-H), 6.99 (dt, ^3J = 7.55, 7.53, ^4J = 0.96 Hz, 1 H, 9-H), 6.87–6.78 (m, 2 H, 2-H/4-H), 4.75–4.48 (m, $^2J_{Pt\text{-}H}$ = 50.05 Hz, 2 H, $H_{ethylene}$), 4.46–4.21 (m, $^2J_{Pt\text{-}H}$ = 54.75 Hz, 2 H, $H_{ethylene}$), 3.47–3.24 (m, 6 H, CH_2), 3.22–3.13 (m, 2 H, CH_2), 3.07–2.40 (m, 6 H, 16-H/17-H), 2.56 (s, 6 H, 21-H/22-H) ppm. ^{195}Pt NMR (85.96 MHz, CD_2Cl_2, 295.0 K): δ = –2849 ppm. ^{13}C NMR (100.56 MHz, CD_2Cl_2, 295.0 K): δ = 163.35 (C-13), 155.58 (C-18), 148.91 (C-1), 147.98 (C-12), 136.34 (C-7), 131.81 (C-8), 131.21 (C-6), 131.11 (C-5), 129.33 (C-11), 127.05 (C-3), 126.77 (C-10), 122.37 (C-2), 121.85 (C-9), 119.78 (C-4), 70.86 (2 C, $C_{ethylene}$), 48.90 (2 C, C-14/C-15), 47.73 (2 C, C-19/C-20), 35.43 (4 C, CH_3) ppm. IR (CsI): $\tilde{\nu}$ = 3012 (w), 2927 (w), 2871 (m), 1635 (s), 1586 (s), 1558 (s), 1502 (w), 1471 (m), 1420 (m), 1390 (m), 1278 (s), 1238 (m), 1150 (w), 1117 (w), 1032 (m), 967 (m), 869 (w), 833 (w), 783 (m), 748 (s), 694 (w), 652 (w), 586 (w), 559 (w), 510 (s), 471 (w) cm^{-1}. Raman (514 nm, 300 mW): λ = 28.2, 39.6, 56.3, 90.9, 149.1, 212.2, 330.2/336.6, 372.2, 396.8, 424.9, 468.3, 488.5, 511.7, 561.5, 605.6, 643.5, 724.4, 739.2, 782.6, 1044.6, 1154.6/1160.5, 1230.2, 1245.5, 1298.8, 1497.0, 1553.9, 1563.7, 1589.4, 1600.3, 1632.8, 3044.3 cm^{-1}. UV/Vis (CH_3CN, $c = 1.56 \times 10^{-5}$ mol L^{-1}): λ (ε) = 269 (10784 L mol^{-1} cm^{-1}) nm. HRMS (FAB$^+$): m/z (%) = 669.1769 (63.4), 670.1799 (81.2), 671.1766 (100.0), 672.1766 (65.8), 673.1758 (60.7) [MH]$^+$. $C_{24}H_{32}Cl_2N_6Pt$ (670.54): calcd. C 42.99, H 4.81, N 12.53; found C 42.60, H 4.77, N 12.23.

Crystal data for [PtCl$_2$(C$_2$H$_4$)(κ^1-**2**)]: $C_{24}H_{32}Cl_2N_6Pt$, M_r = 670.54, $0.30 \times 0.25 \times 0.18$ mm^3, triclinic, space group $P\bar{1}$, a = 9.934(2), b = 10.492(2), c = 13.034(3) Å, α = 101.96(3), β = 95.39(3), γ = 106.01(3)°, V = 1260.9(5) Å^3, Z = 2, $\rho_{calcd.}$ = 1.766 Mg m^{-3}, Mo-K_α radiation (graphite-monochromated, λ = 0.71073 Å), T = 100 K, θ_{range} = 2.08–30.17°. Reflections measured 13245, independent 7327, R_{int} = 0.0388. Final R indices [$I > 2\sigma(I)$]: R_1 = 0.0270, wR_2 = 0.0705.

[PtCl$_2$(C$_2$H$_4$){(*R*)-κ^1-4}]: [PtCl$_2$(C$_2$H$_4$)]$_2$ (77.43 mg, 0.13 mmol, 1 equiv.) dissolved in toluene (9 mL) was added to a solution of (*R*)-**4** in toluene (6 mL). After 30 min the reaction was quenched by reducing the volume of the reaction mixture to around 4 mL and adding PE (40/60, 10 mL). A yellow precipitate was filtered off and washed twice with PE (40/60, 5 mL) to give [PtCl$_2$(C$_2$H$_4$){(*R*)-**4**}] (152.8 mg, 77%) as a light-yellow powder. ^{1}H NMR (399.89 MHz, CD_2Cl_2, 295.1 K): δ = 8.35 (d, ^3J = 8.78 Hz, 1 H, CH), 7.82 (t, ^3J = 7.34, 2 H, CH), 7.74 (d, ^3J = 8.03 Hz, 1 H, CH), 7.69 (d, ^3J = 8.75 Hz, 2 H, CH), 7.34–7.10 (m, 7 H, CH), 4.56–4.40 (m, 2 H, $H_{ethylene}$), 4.32–4.12 (m, 2 H, $H_{ethylene}$), 3.42–2.95 (m, 8 H, CH_2), 2.82 (s, 3 H, CH_3), 2.57 (s, 6 H, CH_3), 2.07 (s, 3 H, CH_3) ppm. ^{195}Pt NMR (85.96 MHz, CD_2Cl_2, 294.8 K): δ = –2853 ppm. ^{13}C NMR (100.56 MHz, CD_2Cl_2, 296.4 K): δ = 156.58, 140.08, 146.39, 134.41 (C_q), 130.86 (CH), 130.36 (C_q), 128.12, 127.35, 126.79, 126.63, 126.21, 125.31, 124.42, 123.84, 123.24 (CH), 69.81 (2 C, $C_{ethylene}$), 48.90 (2 C, CH_2), 47.06 (2 C, CH_2), 35.92 (4C, CH_3) ppm. IR (CsI): $\tilde{\nu}$ = 3041 (w), 2962 (s), 2882 (m), 1630 (s), 1605 (s), 1588 (s), 1553 (sh), 1503 (w), 1482 (w), 1438 (w), 1415 (m), 1383 (m), 1294 (m), 1262 (m), 1092 (s), 1038 (s), 954 (w), 856 (m), 806 (s), 747 (m), 698 (w), 623 (w), 599 (w), 496 (m), 482 (m) cm^{-1}. Raman measurements not possible due to laser beam damage (even for 100 mW and short exposure times). UV/Vis (CH_3CN, $c = 1.23 \times 10^{-5}$ mol L^{-1}): λ (ε) = 352 (3311), 302 (11999), 265 (22597), 243 (24799), 209 (33284 L mol^{-1} cm^{-1}) nm. HRMS (FAB$^+$): m/z (%) = 769.2045 (55.6), 770.2055 (85.8), 771.2028 (100.0), 772.2070 (71.1), 773.2063 (60.3) [MH]$^+$. $C_{32}H_{36}Cl_2N_6Pt$ (770.66): calcd. C 49.87, H 4.71, N 10.90; found C 51.02, H 4.88, N 10.17.

Catalytic Hydrosilylation: Et_3SiH (0.48 mL, 3 mmol) and $Me_3SiC(H)CH_2$ (0.87 mL, 6 mmol) were dissolved in *n*-hexane (30 mL). Then the potential catalyst ([PtCl$_2$(C$_2$H$_4$)(κ^1-**1**)], [PtCl$_2$(C$_2$H$_4$)(κ^1-**2**)] or [PtCl$_2$(C$_2$H$_4$)(κ^1-**4**)], 6×10^{-3} mmol) was added. The reaction (at 25 °C) was followed by GC–MS. For these measurements, 0.1 mL of the reaction mixture was filtered through a silica frit. The product $Et_3SiCH_2CH_2SiMe_3$ was redissolved and removed from the silica with *n*-hexane (2 mL) before being injected into the GC–MS machine.

X-ray Crystallographic Study: Suitable crystals were taken directly from the mother liquor, immersed in perfluorinated polyether oil and fixed on top of a glass capillary. Data were collected with a Nonius–Kappa CCD diffractometer with a low-temperature unit using graphite-monochromated Mo-K_α radiation. The temperature was set to 100 K. The data collected were processed using the standard Nonius software.[42] All calculations were performed using the SHELXT-PLUS software package. Structures were solved by direct methods with the SHELXS-97 program and refined with the SHELXL-97 program.[43,44] Graphical handling of the structural data during solution and refinement was performed with XPMA.[45] Atomic coordinates and anisotropic thermal parameters of non-hydrogen atoms were refined by full-matrix least-squares calculations.

CCDC-790562 (for **2**), -790558 [for (*R*)-**3**], -790561 [for (*R*)-**4**], -790936 (for **5**), -790557 {for [PtCl$_2$(C$_2$H$_4$)(κ^1-**2**)]}, -790559 {for [(**1**H)PtCl$_3$]}, -790560 (for [(**1**H)PdCl$_3$]) contain the supplementary crystallographic data for this paper. These data can be obtained free of charge from The Cambridge Crystallographic Data Centre via www.ccdc.cam.ac.uk/data_request/cif.

Quantum Chemical Calculations: Quantum chemical calculations were carried out with the Gaussian 03[46] and Gaussian 09[47] program package. The B3LYP functional together with the LANL2DZ basis set was used throughout these calculations.

Supporting Information (see footnote on the first page of this article): UV/Vis spectra of **1** and **3**, Raman spectrum of **1**, Raman and IR spectra of **5**, CV curves for **2** and **4** in CH_2Cl_2, calculated structure (B3LYP/6-311G**) of dication $\mathbf{5}^{2+}$, UV/Vis spectrum obtained for the oxidation of **5** with I_2 in CH_3CN, IR spectra of free **2** and the complex [PtCl$_2$(C$_2$H$_4$)(κ^1-**2**), molecular structures of [(**1**H)PdCl$_3$] and [(**1**H)PtCl$_3$], Raman spectra of **2** and [PtCl$_2$(C$_2$H$_4$)(κ^1-**2**)] and gas-phase structures of [PtCl$_2$(C$_2$H$_4$)(κ^1-**2**)], [PtCl$_2$(C$_2$H$_4$)(κ^1-**4**)] and [PtCl$_2$(C$_2$H$_4$)(κ^1-**1**)].

Acknowledgments

Continued financial support from the Deutsche Forschungsgemeinschaft (DFG) is gratefully acknowledged.

[1] a) R. Noyori, *Chem. Soc. Rev.* **1989**, *18*, 187–208; b) R. Noyori, H. Takaya, *Acc. Chem. Res.* **1990**, *23*, 345–350; c) S. Otsuka, K. Tani, *Synthesis* **1991**, 665–680; d) C. Rosini, L. Franzini, A. Raffaelli, P. Salvadori, *Synthesis* **1992**, 503–517; e) S. Akutagawa, *Appl. Catal. A* **1995**, *128*, 171–207; f) R. Noyori, *Adv. Synth. Catal.* **2003**, *345*, 15–32.

[2] A. Miyashita, A. Yasuda, H. Takaya, K. Toriumi, T. Ito, T. Souchi, R. Noyori, *J. Am. Chem. Soc.* **1980**, *102*, 7932–7934.

[3] a) A. Miyashita, H. Takaya, T. Souchi, R. Noyori, *Tetrahedron* **1984**, *40*, 1245–1253; b) K. J. Brown, M. S. Berry, K. C. Waterman, D. Lingenfelter, J. R. Murdoch, *J. Am. Chem. Soc.* **1984**, *106*, 4717–4723.

[4] T. Ishikawa, *Superbases for Organic Synthesis*, John Wiley & Sons, New York, **2009**, pp. 93–143.

[5] a) F. T. Edelmann, *Adv. Organomet. Chem.* **2008**, *57*, 183–352; b) F. T. Edelmann, *Chem. Soc. Rev.* **2009**, *38*, 2253–2268.

[6] a) M. P. Coles, *Dalton Trans.* **2006**, 985–1001; b) M. P. Coles, *Chem. Commun.* **2009**, 3659–3676; c) M. P. Coles, P. J. Aragón-Sáez, S. H. Oakley, P. B. Hitchcock, M. G. Davidson, Z. B. Maksić, R. Vianello, I. Leito, I. Kaljurand, D. C. Apperley, *J. Am. Chem. Soc.* **2009**, *131*, 16858–16868.

[7] a) F. A. Cotton, J. H. Matonic, C. A. Murillo, *J. Am. Chem. Soc.* **1997**, *119*, 7889–7890; b) F. A. Cotton, L. M. Daniels, C. A. Murillo, D. J. Timmons, *Chem. Commun.* **1997**, 1449–1450; c) F. A. Cotton, N. E. Gruhn, J. Gu, P. Huang, D. L. Lichtenberger, C. A. Murillo, L. O. Van Dorn, C. C. Wilkinson, *Science* **2002**, *298*, 1971–1974; d) F. A. Cotton, J. Gu, C. A. Murillo, D. J. Timmons, *J. Am. Chem. Soc.* **1998**, *120*, 13280–13281; e) F. A. Cotton, J. P. Donahue, D. L. Lichtenberger, C. A. Murillo, D. Villagrán, *J. Am. Chem. Soc.* **2005**, *127*, 10808–10809; F. A. Cotton, N. S. Dalal, P. Huang, S. A. Ibragimov, C. A. Murillo, P. M. B. Piccoli, C. M. Ramsey, A. J. Schultz, X. Wang, Q. Zhao, *Inorg. Chem.* **2007**, *46*, 1718–1726.

[8] a) C. Würtele, E. Gaoutchenova, K. Harms, M. C. Holthausen, J. Sundermeyer, S. Schindler, *Angew. Chem.* **2006**, *118*, 3951–3954; *Angew. Chem. Int. Ed.* **2006**, *45*, 3867–3869; b) D. Maiti, D.-H. Lee, K. Gaoutchenova, C. Würtele, M. C. Holthausen, A. A. N. Sarjeant, J. Sundermeyer, S. Schindler, K. D. Karlin, *Angew. Chem.* **2007**, *120*, 88–91; *Angew. Chem. Int. Ed.* **2007**, *47*, 82–85; c) M. P. Lanci, V. V. Smirnov, C. J. Cramer, E. V. Gauchenova, J. Sundermeyer, J. P. Roth, *J. Am. Chem. Soc.* **2007**, *129*, 14697–14709; d) D. Maiti, D.-H. Lee, K. Gaoutchenova, C. Würtele, M. C. Holthausen, A. A. N. Sarjeant, J. Sundermeyer, S. Schindler, K. D. Karlin, *Angew. Chem.* **2008**, *120*, 88–91; *Angew. Chem. Int. Ed.* **2008**, *47*, 82–85.

[9] S. Herres-Pawlis, *Nachr. Chem.* **2009**, *57*, 20–23.

[10] a) S. Pohl, M. Harmjanz, J. Schneider, W. Saak, G. Henkel, *J. Chem. Soc., Dalton Trans.* **2000**, 3473–3479; b) D. Petrovic, L. M. R. Hill, P. G. Jones, W. B. Tolman, M. Tamm, *Dalton Trans.* **2008**, 887–894; c) S.-A. Filimon, C. G. Hrib, S. Randoll, I. Neda, P. G. Jones, M. Tamm, *Z. Anorg. Allg. Chem.* **2010**, *636*, 691–699.

[11] a) C. J. Carmalt, A. C. Newport, S. A. O'Neill, I. P. Parkin, A. J. P. White, D. J. Williams, *Inorg. Chem.* **2005**, *44*, 615–619; b) D. Rische, H. Parala, E. Gemel, M. Winter, R. A. Fischer, *Chem. Mater.* **2006**, *18*, 6075–6082; c) A. P. Milanov, R. Bhakta, A. Baunemann, H.-W. Becker, R. Thomas, P. Ehrhart, M. Winter, A. Devi, *Inorg. Chem.* **2006**, *45*, 11008–11018; d) J. P. Coyle, W. H. Monillas, G. P. A. Yap, S. T. Barry, *Inorg. Chem.* **2008**, *47*, 683–689; e) J. P. Coyle, W. H. Monillas, G. P. A. Yap, S. T. Barry, *Inorg. Chem.* **2008**, *47*, 683–689; f) A. Baunemann, D. Bekermann, T. B. Thiede, H. Parala, M. Winter, C. Gemel, R. A. Fischer, *Dalton Trans.* **2008**, *28*, 3715–3722; g) A. P. Milanov, T. B. Thiede, A. Devi, R. A. Fischer, *J. Am. Chem. Soc.* **2009**, *131*, 17062–17063; h) S. E. Potts, C. J. Carmalt, C. S. Blackman, F. Abou-Chahine, D. Pugh, H. O. Davies, *Organometallics* **2009**, *28*, 1838–1844; i) A. P. Milanov, T. B. Thiede, A. Devi, R. A. Fischer, *J. Am. Chem. Soc.* **2009**, *131*, 17062–17063; j) A. P. Milanov, T. Toader, H. Parala, D. Barreca, G. A. Davide, C. Bock, H.-W. Becker, D. K. Ngwashi, R. Cross, S. Paul, U. Kunze, R. A. Fischer, A. Devi, *Chem. Mater.* **2009**, *21*, 5443–5455; k) T. Chen, W. Hunks, P. S. Chen, C. Xu, A. G. Di Pasquale, A. L. Rheingold, *Organometallics* **2010**, *29*, 501–504; l) A. P. Milanov, K. Xu, A. Laha, E. Bugiel, R. Ranjith, D. Schwendt, H. J. Osten, H. Parala, R. A. Fischer, A. Devi, *J. Am. Chem. Soc.* **2010**, *132*, 36–37.

[12] a) U. Wild, P. Roquette, E. Kaifer, J. Mautz, H. Wadepohl, H.-J. Himmel, *Eur. J. Inorg. Chem.* **2008**, 1248–1257; b) A. Peters, U. Wild, O. Hübner, E. Kaifer, J. Mautz, H.-J. Himmel, *Chem. Eur. J.* **2008**, *14*, 7813–7821; c) U. Wild, O. Hübner, A. Maronna, M. Enders, E. Kaifer, H. Wadepohl, H.-J. Himmel, *Eur. J. Inorg. Chem.* **2008**, 4440–4447; d) D. Domide, C. Neuhäuser, E. Kaifer, H. Wadepohl, H.-J. Himmel, *Eur. J. Inorg. Chem.* **2009**, 2170–2178; e) A. Peters, C. Trumm, M. Reinmuth, D. Emeljanenko, E. Kaifer, H.-J. Himmel, *Eur. J. Inorg. Chem.* **2009**, 3791–3800; f) M. Reinmuth, U. Wild, E. Kaifer, M. Enders, H. Wadepohl, H.-J. Himmel, *Eur. J. Inorg. Chem.* **2009**, 4795–4808; g) D. Emeljanenko, A. Peters, N. Wagner, J. Beck, E. Kaifer, H.-J. Himmel, *Eur. J. Inorg. Chem.* **2010**, 1839–1846; h) C. Trumm, O. Hübner, E. Kaifer, H.-J. Himmel, *Eur. J. Inorg. Chem.* **2010**, 3102–3108.

[13] U. Köhn, W. Günther, H. Görls, E. Anders, *Tetrahedron: Asymmetry* **2004**, *15*, 1419–1426.

[14] U. Köhn, M. Schulz, H. Görls, E. Anders, *Tetrahedron: Asymmetry* **2005**, *16*, 2125–2131.

[15] S. J. Angyal, W. K. Warburton, *J. Chem. Soc.* **1951**, 2492–2494.

[16] P. Roquette, A. Maronna, A. Peters, E. Kaifer, H.-J. Himmel, Ch. Hauf, V. Herz, E.-W. Scheidt, W. Scherer, *Chem. Eur. J.* **2010**, *16*, 1336–1350.

[17] V. Raab, J. Kipke, R. M. Gschwind, J. Sundermeyer, *Chem. Eur. J.* **2002**, *8*, 1682–1693.

[18] R. W. Alder, P. S. Bowman, W. R. S. Steele, D. R. Winterman, *Chem. Commun. (London)* **1968**, 723–724.

[19] T. Yamasaki, N. Ozaki, Y. Saika, K. Ohta, K. Goboh, F. Nakamura, M. Hashimoto, S. Okeya, *Chem. Lett.* **2004**, *33*, 928–929.

[20] U. Wild, O. Hübner, A. Maronna, M. Enders, E. Kaifer, H. Wadepohl, H.-J. Himmel, *Eur. J. Inorg. Chem.* **2008**, 4440–4447.

[21] A. Peters, E. Kaifer, H.-J. Himmel, *Eur. J. Org. Chem.* **2008**, 5907–5914.

[22] A. Peters, C. Trumm, M. Reinmuth, D. Emeljanenko, E. Kaifer, H.-J. Himmel, *Eur. J. Inorg. Chem.* **2009**, 3791–3800.

[23] D. Emeljanenko, A. Peters, V. Vitske, E. Kaifer, H.-J. Himmel, *Eur. J. Inorg. Chem.* **2010**, 4783–4789.

[24] V. Vitske, C. König, E. Kaifer, O. Hübner, H.-J. Himmel, *Eur. J. Inorg. Chem.* **2010**, 115–126.

[25] T. A. Taton, P. Chen, *Angew. Chem.* **1996**, *108*, 1098–1100; *Angew. Chem. Int. Ed. Engl.* **1996**, *35*, 1011–1013.

[26] R. D. Richardson, T. Wirth, *Chem. Unserer Zeit* **2008**, *42*, 186–191.

[27] P. Pruszynski, K. T. Leffek, B. Borecka, T. S. Cameron, *Acta Crystallogr., Sect. C* **1992**, *48*, 1638–1641.

[28] A. Almenningen, O. Bastiansen, L. Fernholt, B. N. Cyvin, S. J. Cyvin, S. Samdal, *J. Mol. Struct.* **1985**, *128*, 59–76.

[29] a) E. P. Carr, H. Stücklen, *J. Chem. Phys.* **1936**, *4*, 760–768; b) F. Almasy, H. Lämmel, *Helv. Chim. Acta* **1950**, *33*, 2092–2100.

[30] a) B. Williamson, W. H. Rodebush, *J. Am. Chem. Soc.* **1941**, *63*, 3018–3025; b) E. Marcus, W. M. Lauer, R. T. Arnold, *J. Am. Chem. Soc.* **1958**, *80*, 3742–3745.

[31] a) R. A. Friedel, M. Orchin, L. Reggel, *J. Am. Chem. Soc.* **1948**, *70*, 199–204; b) J. C. Del Riccio, F. Zhang, A. R. Lacey, S. H. Kable, *J. Phys. Chem. A* **2000**, *104*, 7442–7451.

[32] F. Zhang, G. B. Bacskay, S. H. Kable, *J. Phys. Chem. A* **2004**, *108*, 172–184.

[33] J. L. Del Riccio, F. Zhang, A. R. Lacey, S. H. Kable, *J. Phys. Chem. A* **2000**, *104*, 7442–7451.

[34] I. R. Gould, D. Ege, J. E. Moser, S. Farid, *J. Am. Chem. Soc.* **1990**, *112*, 4290–4301.

[35] L. Manceron, L. Andrews, *J. Phys. Chem.* **1986**, *90*, 4514–4528.
[36] For an alternative analysis, see: E. B. Burgina, E. N. Yurchenko, *J. Mol. Struct.* **1984**, *116*, 17–27.
[37] N. Hebben, H.-J. Himmel, G. Eickerling, C. Herrmann, M. Reiher, V. Herz, M. Presnitz, W. Scherer, *Chem. Eur. J.* **2007**, *13*, 10078–10087.
[38] P. A. Dub, O. A. Filippov, N. V. Belkova, M. Rodriguez-Zubiri, R. Poli, *J. Phys. Chem. A* **2009**, *113*, 6348–6355.
[39] D. B. Powell, J. G. V. Scott, N. Sheppard, *Spectrochim. Acta Part A* **1972**, *28*, 327–335.
[40] M. A. M. Meester, D. J. Stufkens, K. Vrieze, *Inorg. Chim. Acta* **1977**, *21*, 251–258.
[41] M. Amirnasr, G. Kickelbick, S. Dehghanpour, *Helv. Chim. Acta* **2006**, *89*, 274–284.
[42] *DENZO-SMN, Data processing software*, Nonius, **1998** (http://www.nonius.com).
[43] a) G. M. Sheldrick, *SHELXS-97*, *Program for Crystal Structure Solution*, University of Göttingen, Göttingen, **1997** (http://shelx.uni-ac.gwdg.de/SHELX/index.html); b) G. M. Sheldrick, *SHELXL-97*, *Program for Crystal Structure Refinement*, University of Göttingen, Göttingen, **1997** (http://shelx.uni-ac.gwdg.de/SHELX/index.html).
[44] *International Tables for X-ray Crystallography*, vol. 4, Kynoch Press, Birmingham, **1974**, .
[45] L. Zsolnai, G. Huttner, *XPMA*, University of Heidelberg, Heidelberg, **1994** (http://www.uni-heidelberg.de/institute/fak12/AC/huttner/software/software.html).
[46] M. J. Frisch, G. W. Trucks, H. B. Schlegel, G. E. Scuseria, M. A. Robb, J. R. Cheeseman, V. G. Zakrzewski, J. A. Montgomery Jr., R. E. Stratmann, J. C. Burant, S. Dapprich, J. M. Millam, A. D. Daniels, K. N. Kudin, M. C. Strain, O. Farkas, J. Tomasi, V. Barone, M. Cossi, R. Cammi, B. Mennucci, C. Pomelli, C. Adamo, S. Clifford, J. Ochterski, G. A. Petersson, P. Y. Ayala, Q. Cui, K. Morokuma, D. K. Malick, A. D. Rabuck, K. Raghavachari, J. B. Foresman, J. Cioslowski, J. V. Ortiz, B. B. Stefanov, G. Liu, A. Liashenko, P. Piskorz, I. Komaromi, R. Gomperts, R. L. Martin, D. J. Fox, T. Keith, M. A. Al-Laham, C. Y. Peng, A. Nanayakkara, C. Gonzalez, M. Challacombe, P. M. W. Gill, B. Johnson, W. Chen, M. W. Wong, J. L. Andres, C. Gonzalez, M. Head-Gordon, E. S. Replogle, J. A. Pople, *Gaussian 03*, Gaussian Inc., Pittsburgh, PA, **1998**.
[47] M. J. Frisch, G. W. Trucks, H. B. Schlegel, G. E. Scuseria, M. A. Robb, J. R. Cheeseman, G. Scalmani, V. Barone, B. Mennucci, G. A. Petersson, H. Nakatsuji, M. Caricato, X. Li, H. P. Hratchian, A. F. Izmaylov, J. Bloino, G. Zheng, J. L. Sonnenberg, M. Hada, M. Ehara, K. Toyota, R. Fukuda, J. Hasegawa, M. Ishida, T. Nakajima, Y. Honda, O. Kitao, H. Nakai, T. Vreven, J. A. Montgomery, Jr., J. E. Peralta, F. Ogliaro, M. Bearpark, J. J. Heyd, E. Brothers, K. N. Kudin, V. N. Staroverov, R. Kobayashi, J. Normand, K. Raghavachari, A. Rendell, J. C. Burant, S. S. Iyengar, J. Tomasi, M. Cossi, N. Rega, J. M. Millam, M. Klene, J. E. Knox, J. B. Cross, V. Bakken, C. Adamo, J. Jaramillo, R. Gomperts, R. E. Stratmann, O. Yazyev, A. J. Austin, R. Cammi, C. Pomelli, J. W. Ochterski, R. L. Martin, K. Morokuma, V. G. Zakrzewski, G. A. Voth, P. Salvador, J. J. Dannenberg, S. Dapprich, A. D. Daniels, O. Farkas, J. B. Foresman, J. V. Ortiz, J. Cioslowski, D. J. Fox, *Gaussian 09*, Revision A.02, Gaussian Inc., Wallingford, CT, **2009**.

Received: September 15, 2010
Published Online: January 26, 2011

